OPEN ACCESS
Journal of Innovative Optical Health Sciences
Vol. 15, No. 1 (2022) 2242002 (13 pages)

DOI: 10.1142/S1793545822420020

World Scientific
www.worldscientific.com

Laser speckle contrast imaging for monitoring of acute pancreatitis at ischemia–reperfusion injury of the pancreas in rats

P. A. Dyachenko (Timoshina)[*,†,‖], A. N. Bashkatov[*,†], D. A. Alexandrov[‡], V. I. Kochubey[*] and V. V. Tuchin[†,§,¶]

[*]*Saratov State University, Saratov, Russia*

[†]*Laboratories of Biophotonics and Laser Molecular Imaging and Machine Learning National Research Tomsk State University, Tomsk, Russia*

[‡]*Saratov State Medical University, Saratov, Russia*

[§]*Institute of Precision Mechanics and Control, Russian Academy of Sciences, Russia*

[¶]*A.N. Bach Institute of Biochemistry, Research Center of Biotechnology of the Russian Academy of Sciences Moscow, Russia*

[‖]*timoshina2906@mail.ru*

Received 30 May 2021
Accepted 11 October 2021
Published 19 November 2021

The influence of ischemia–reperfusion (I/R) action on pancreatic blood flow (PBF) and the development of acute pancreatitis (AP) in laboratory rats is evaluated *in vivo* by using the laser speckle contrast imaging (LSCI). Additionally, the optical properties in norm and under condition of AP in rats were assessed using a modified integrating sphere spectrometer and inverse Monte Carlo (IMC) software. The results of the experimental study of microcirculation of the pancreas in 82 rats in the ischemic model are presented. The data obtained confirm the fact that local ischemia and changes in the blood flow velocity of the main vessels cause and provoke acute pancreatitis.

Keywords: Laser speckles; contrast of speckle images; adaptive algorithm; microcirculation; blood flow; acute pancreatitis; pancreas; rats; optical properties; integrating sphere spectroscopy.

1. Introduction

Acute pancreatitis (AP) is a common disease. Nearly, 75% of patients suffer from a mild edematous form of pancreatitis. In 25% of patients, a severe degree of the disease with a mortality rate of 30–60% can be expected.[1] In AP, an important role in the progression of the disease is reduction of blood flow and alterations of microvascular integrity, resulting in impaired tissue oxygenation.[1] The crucial trigger of AP is the intra-pancreatic activation of trypsinogen to trypsin.[1] Further, there is a release of local mediators (cytokines, vasoactive substances, and free oxygen radicals) and subsequently the development of microcirculatory disturbances and the activation of leukocytes and their infiltration into the tissue.[1] At present, the deterioration of microcirculation is seen as the most important pacemaker in the progression to a necrotizing pancreatitis. In addition to its potential role, severe pancreatic ischemia can play a pathogenetic role in the initiation of acute pancreatitis.[1]

One of the main roles in the pathophysiological development of pancreatitis, leading to tissue hypoxia, plays microcirculatory disorders. In the 1980s, studies were conducted showing the high sensitivity of the pancreas to a decrease of perfusion and ischemia and revealing a direct relationship between pathological changes of pancreas tissues and a repeated disturbance of the blood flow.[2] Also, there is an increasing evidence that ischemia alone may be the primary cause of pancreatitis or may be the exacerbating promoter for the progression from edematous to necrotizing pancreatitis.[1] Studies of Warshaw *et al.*[3,4] are of particular interest because they present clinical evidence of high sensitivity of the pancreas to a decrease of perfusion and ischemia and show, along with other studies, that primary or secondary disturbances of blood flow in the pancreas cause pathological changes in it. In clinical studies, there was evidence that ischemia during cardiopulmonary bypass triggered AP, and it was found in up to 25% of autopsies of patients who died after shock. Also, the hypothesis that the manifestation of microvascular injury in AP involves ischemia–reperfusion (I/R)-associated events is supported by the study of Menger *et al.*,[1,5] who analyzed the pancreatic microcirculation of rats during post-ischemic reperfusion by use of intravital fluorescence microscopy. The functional and histomorphological alterations in this study were similar to the alterations seen in edematous pancreatitis.[1]

Currently, the methods based on dynamic light scattering,[12] as well as on principles of low-coherence optical coherence tomography (OCT), and the so-called Doppler OCT (DOCT)[6–8] are actively used to determine blood flow parameters. Also, one of the prospective methods for the assessment of blood flow is the laser speckle contrast imaging (LSCI).[9–15]

In this paper, we have tested the experimental model of I/R of the pancreas tissue by simulating a reversible impaired blood flow in the vessels of the pancreas; since whatever the specific pathophysiological causes of pancreatitis, the central pathogenetic role in its progression, with consequences in the form of tissue hypoxia and (or) anoxia, belongs to microcirculatory disorders. Also, an important problem of urgent surgery is the development of effective methods for microcirculation monitoring of the abdominal cavity at AP and its complications. Changes of pancreas tissue in conditions of development of pancreatitis are characterized by slowing down the linear velocity of pancreatic blood flow (PBF) due to vasculature stasis, red blood cell (RBC) aggregation, and vascular permeability increase. In this regard, it is important to determine and monitor the physiological parameters of the blood flow.

2. Materials and Methods

2.1. *Speckle contrast imaging of pancreas*

In this study, for hemodynamic monitoring, we used the speckle contrast method, which is one of the laser speckle imaging methods. This simple and highly effective technique for visualization of blood flow was proposed in the mid-90s of the last century and was named laser speckle contrast analysis (LASCA).[9,16–18] It is based on the similarity of the values of statistical moments of the spatio-temporal intensity fluctuations of ergodic and statistically homogeneous speckle fields, estimated by time and spatial averaging.[9,11]

LASCA is based on the calculation of contrast of time-averaged dynamic speckles in dependence on the exposure time at the registration of the speckle-modulated images. The local estimation of the contrast K_k is carried out in a fixed exposure time

and in areas with a given number of speckles that makes it possible to visualize tissue regions with essentially different velocities of the scatterers:[9–12]

$$K_k = \sigma_{Ik}/\bar{I}_k, \tag{1}$$

where k is the number of frames in a sequence of speckle-modulated images and $\bar{I}_k$ and σ_{Ik} are averaged over the analyzed frame scattered light intensity and the root mean square (rms) value of the fluctuation component of the pixel's brightness, respectively:

$$\bar{I}_k = (1/MN)\sum_{m=1}^{M}\sum_{n=1}^{N} I_k(m,n), \tag{2}$$

$$\sigma_{Ik} = \sqrt{(1/MN)\sum_{m=1}^{M}\sum_{n=1}^{N}\{I_k(m,n) - \bar{I}_k\}^2}, \tag{3}$$

where M and N are the number of pixels in rows and columns of the analyzed area of the frame, respectively; $I_k(m,n)$ is the brightness of the (m,n) pixel of the k-frame.

The problem of quantitative velocity measurements is associated with understanding the interconnection between the contrast of speckles and the velocity of scattering centers (or velocity distribution).[19–21] The higher velocity, the faster fluctuations, and the lower contrast for the fixed exposure time are measured. Depending on the type of the studied motion, different models may be used. For the Lorentz velocity distribution, corresponding to Brownian motion of particles, the equation takes the following form:[22,23]

$$K = \frac{\sigma_s}{\langle I\rangle} = \left[\frac{\tau_c}{2T}\left\{1 - \exp\left(-\frac{2T}{\tau_c}\right)\right\}\right]^{1/2}. \tag{4}$$

As for the Gaussian velocity distribution, the equation takes the following form:

$$K = \frac{\sigma_s}{\langle I\rangle} = \left[\frac{\tau_c}{2T}\left\{\sqrt{2\pi}\mathrm{erf}\left(\frac{\sqrt{2}T}{\tau_c}\right) - \frac{\tau_c}{T}\left(1 - \exp\left(-\frac{2T}{\tau_c}\right)^2\right)\right\}\right]^{1/2}. \tag{5}$$

It is worth noting that this equation is characteristic to directed flows.[24] These equations relate the speckle contrast and the correlation time τ_c for a given time of averaging T.

Due to uncertainties caused by the different factors, namely, the form of the velocity distribution of scattering particles, multiple scattering, size of the particles (RBCs), shape of scatterers, non-Newtonian flow of the liquid, non-Gaussian statistics due to small number of scatterers, etc.,[24] one should rely to appropriate calibration using dynamic phantoms of tissues rather than to absolute measurements.

The simplest approach leads to a characteristic velocity υ_c defined as follows:[23–25]

$$\upsilon_c = \lambda/2\pi a\tau_c, \tag{6}$$

where λ is the source wavelength and a is the normalization factor which depends on the parameters of a Gaussian curve from Eq. (5) and the scattering properties of biological tissue or phantom. Calibration procedure described earlier[26,27] allowed us to determine the value of this coefficient as ~ 0.24. In this regard, we introduced the concept of "reduced" velocity using Eqs. (5) and (6) to process phantom experimental data for contrast K at the particular exposure time of the camera T for the range of physiological velocities. "Reduced" velocity υ' can be associated with the velocity of blood flow determined from the speckle contrast K measurements in the further assessment of blood circulation in *in vivo* studies. The results were presented as mean values ±standard deviation (SD), and the differences were compared using the Student's t-test for unpaired data. The differences were considered statistically significant when $p < 0.05$.

To perform the measurements and calculate the contrast, we developed a program in the LabVIEW 8.5 environment (National Instruments, USA) that allows for real-time recording of the intensity distribution of the speckle field with the rate of 100 frames per second and calculation of the mean contrast or its spatial distribution using Eq. (1) with parallel imaging in the region chosen by the operator.[28]

The experimental setup for microcirculation monitoring is shown in Fig. 1.

The setup allowed for recording images of the same fragment of the sample both in coherent light (illumination by a laser) and in incoherent one (illumination by a light emitting diode (LED)) without mechanical rearrangement. The speckle imaging was provided by a single-mode (uniphase) He–Ne laser GN-5P (Russia) with a wavelength of 632.8 nm. The monochrome CMOS camera (Basler a602f, number of pixels in the matrix 656×491, pixel size $9.9 \times 9.9\,\mu$m, 8 bit per pixel) with the fixed exposure time of 20 ms, combined with the

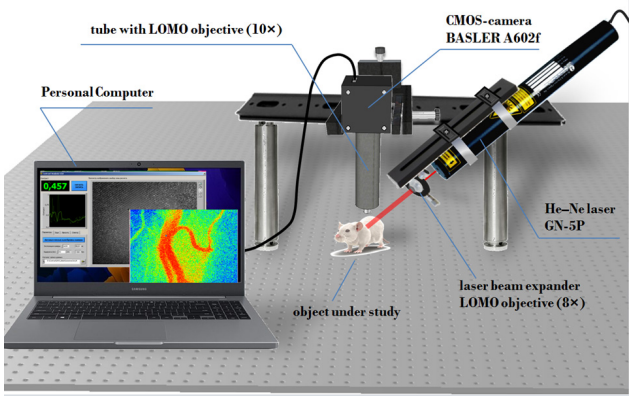

Fig. 1. The scheme of the experimental setup for measurement of blood microcirculation of rat's pancreas.

LOMO objective (10×, St. Petersburg, Russia), was used as a detector.

2.2. *Animal models*

In studies of PBF, 60 animals were examined. Under general anesthesia solution Zoletil 0.2 mL, laparoscopy was performed. Then, the changes of PBF were evaluated. The experiments were carried out in two stages. The first stage included control measurements of microcirculation in the pancreas; 20 animals were used that were divided into two groups (Table 1).

The second stage is the analysis of the effect of complete ischemia of different durations and subsequent reperfusion on the development of pathology in the pancreas of rats. The intensity of microhemodynamics in the course of experiments was changed by artificially created local ischemia as a result of the overcompression (occlusion) of the corresponding pancreatic main blood vessels for different time intervals. The animal was placed under the optical system to visualize the ROI and record PBF within it. Clamping of the vessel was performed in parallel with the recording of blood flow. After clamping, the blood flow was recorded again. After

Table 1. Groups of animals of the first stage of studies of the pancreas.

Group 1	Measurements of PBF were carried out during the first minute, then after 5 min and 20 min, and one day after the start of the experiment.
Group 2	Measurements of PBF were carried out during the first minute, then after 5 min and 20 min, and five days after the start of the experiment.

Table 2. Groups of animals of the second stage of studies of the pancreas.

Group 1	Measurements of PBF were carried out before ischemia, at the time of 5 min-ischemia, and one day after the start of the experiment.
Group 2	Measurements of PBF were carried out before ischemia, at the time of 5 min-ischemia, and 5 days after the start of the experiment.
Group 3	Measurements of PBF were carried out before ischemia, at the time of 20 min-ischemia, and one day after the start of the experiment.
Group 4	Measurements of PBF were carried out before ischemia, at the time of 20 min-ischemia, and 5 days after the start of the experiment.

the data recording was completed, the experiment was stopped and the organic complex was placed in the abdominal cavity. The postoperative wound was sutured. For this stage, 40 laboratory rats divided into four groups were used (Table 2).

After carrying out all the studies *in vivo*, the animal was withdrawn from the experiment; within an hour, samples of pancreatic tissues were taken and the optical properties of the tissues were analyzed.

All procedures with animals were performed in strict accordance with "Rules for Conducting Qualitative Clinical Trials in the Russian Federation" (approved by the Ministry of Health of the Russian Federation and enacted on January 1, 1999), appendix 3 to Order No. 755 of the Ministry of Health of the USSR of 10.08.77, the provisions of WMA Declaration of Helsinki (2000) and the recommendations contained in the European Community Directives (No. 86/609EC).

2.3. *Histological analysis*

The material for histological studies was fixed in a 10% formalin solution, then dehydrated with a set of alcohols of increasing concentration, and filled with paraffin. Sections of 5–10 μm thickness were prepared using a sledge microtome with a lifting object holder on an inclined plane. Sections were stained with hematoxylin and eosin.

2.4. *Measurement of the optical properties of the pancreas*

For the measurements, 20 pancreas samples were used: 10 control samples and 10 samples after modeling 20 min ischemia later five days after beginning the experiment. To measure the thickness,

the samples were placed between two slides; measurements were made by a micrometer at several points. On average, the thickness of the samples was 1 ± 0.11 mm with the accuracy of each measurement of $\pm 10\,\mu$m. Measurement of optical properties of tissue samples (the diffuse reflectance, total, and collimated transmittance) was performed in the spectral range of 350–2500 nm on a spectrophotometer LAMBDA 950 (PerkinElmer, USA) with an integrating sphere. The beam size of the light incident on the sample during the diffuse reflectance and total transmittance measurements was 1.4 mm; the scan rate was 5 nm/s. To measure the collimated transmittance, we used a specially designed add-on device, which consisted of a holder to fix a tissue sample and a system of four diaphragms (two diaphragms in a reference channel and two in a sample (measuring) channel) with a diameter of 2 mm each. All measurements were performed at room temperature ($\sim 20^{\circ}$C). The inverse Monte Carlo (IMC) method described in detail in Refs. 29 and 30 was used for determination of the absorption coefficient (μ_a), the reduced scattering coefficient ($\mu\prime_s$), the scattering coefficient (μ_s), and the scattering anisotropy factor (g) of a tissue from the measured values of the total and collimated transmittance and the diffuse reflectance.

3. Results and Discussion

3.1. *Speckle contrast imaging of pancreas*

Images of a pancreatic vessel (diameter 280 m) in coherent light (630 nm) and the calculated speckle images contrast in diferent states of PBF velocity are presented in Fig. 2. Figure 3 shows the results of a control group of animals, where PBF measurements were carried out at the first minute, at 5 and 20 min of the study and also a day after the start of the experiment (a), and on the 5th day after the start of the experiment (b).

Some decrease in the velocity of PBF (perfusion) at the beginning of the experiment is due to the influence of factors associated with the removal of the organ from the abdominal cavity. However, these changes are not statistically significant.

In Fig. 4, the experimental data obtained in the study of the blood microcirculation in pancreas after local ischemia are presented. The PBF was

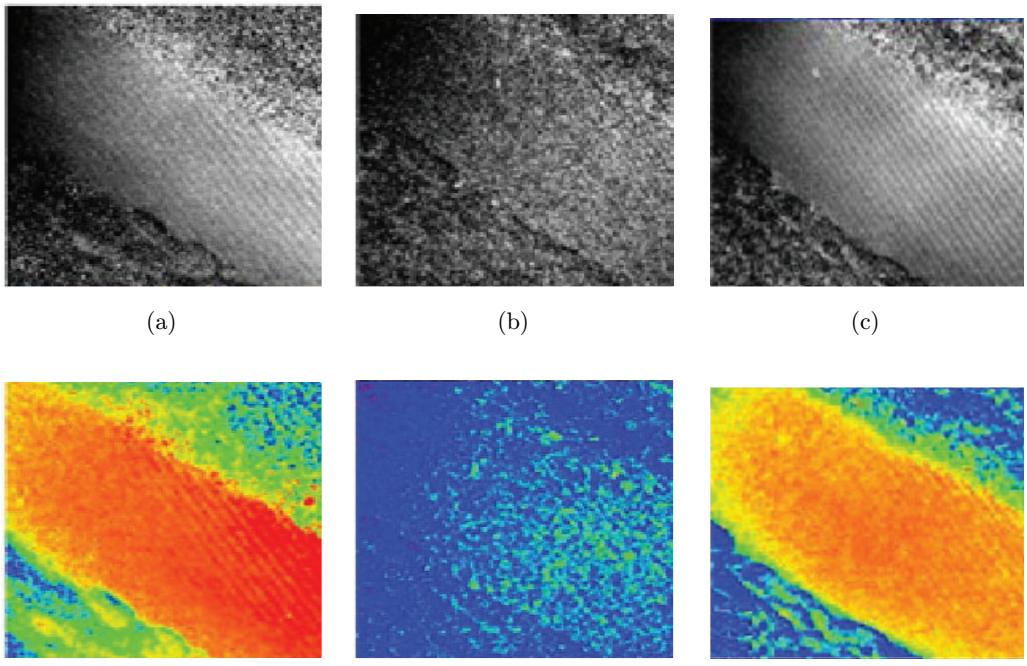

Fig. 2. Images of a pancreatic vessel (diameter 280 μm) in coherent light (630 nm) (a), (b) and the calculated speckle image contrast (1–0) (d)–(f) in different states of PBF velocity: (a), (d) normal, (b), (e) 20 min ischemia (this image was taken at 20 seconds of speckle images recording from the beginning of clamping), (c), (f) reperfusion (this image was taken at 20 s of speckle image recording after the completion of the occlusion of the great pancreatic artery).

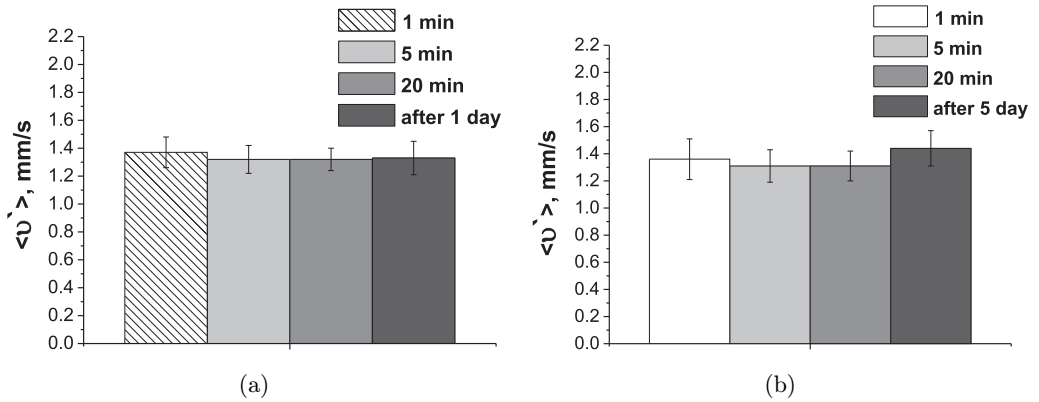

Fig. 3. The reduced blood flow velocity in the pancreatic vessels of rats in control groups.

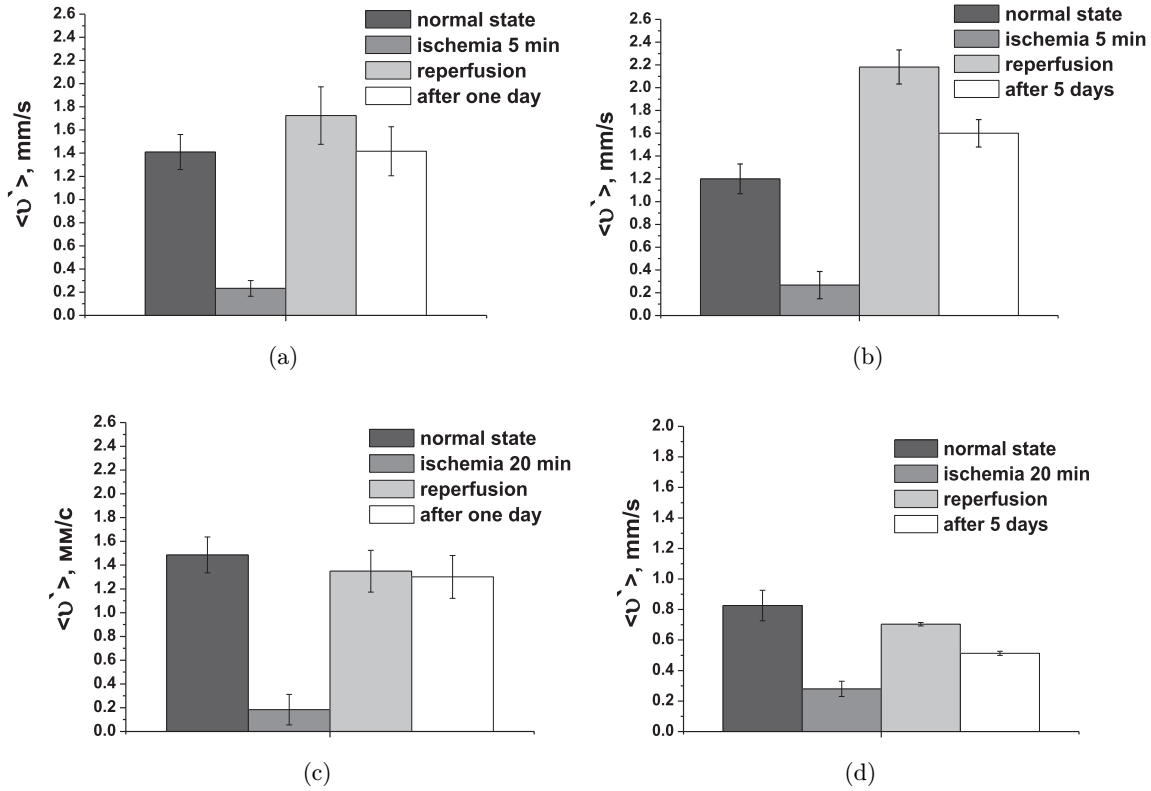

Fig. 4. The PBF measured at different states of the experimental animals with ischemia 5 min (a), (b) were examined immediately after the action, 1 day later (a), and 5 day later (b) and with ischemia 20 min (c), (d) were examined immediately after the action, 1 day later (c), and 5 days later (d).

studied at different states of the experimental animal: Normal functional state (free blood flow), at the time of ischemia and after the ischemia. Time periods of cross-clamping of 5 min and 20 min were examined immediately after the action, 1 day later and 5 days later.

The data values for the normal state differ between the groups; this is due to the variation in the diameter of the studied vessels of the pancreas; in this case, in group 4, the diameter of the studied vessels varied within 150–280 μm, while in the other groups, the diameter was 60–180 μm. In the last groups of animals studied (ischemia 20 min), there was no pronounced increase of PBF velocity during reperfusion, which may have been caused by strong structural changes with prolonged ischemia. At the

(a) (b) (c)

Fig. 5. Photos of the pancreas depending on the functional state: normal state (a), one day after modeling 20 min ischemia, (b) and 5 days after modeling 20 min ischemia (c).

same time, in the group 4 of animals, a decrease in the blood flow rate was registered on the 5th day after the start of the experiment. Figure 5 shows the photographs of the pancreas, depending on the functional state of the pancreas.

Figure 5(c) clearly shows the presence of the organ edema. Reperfusion of ischaemic and hypoxaemic tissues results in locally increased permeability of vessels and organ edema associated with neutrophil accumulation in microcirculation.[31] Reduced blood flow velocity in the pancreas of animals in the group number 5 (20 min ischemia, 5 days after the start of the experiment) can be due to the interaction of neutrophils and endothelial cells, leading to microcirculation impairment. Cytokines produced by neutrophils, monocytes, and lymphocytes cause damage to the endothelium of the vascular wall, slow blood flow, and activate coagulation hemostasis. Decreased blood supply to the organ leads to dysfunction of intracellular organelles, which can activate lysosomal and digestive enzymes to initiate self-healing and damage to pancreatic tissue.[31] Then, leukocytes are activated with their diapedesis in the focus of inflammation. These processes occur during the development of AP. The analysis of microhemodynamic changes in the pancreatic vessels of laboratory rats with alloxan diabetes carried out by speckle-contrast imaging has also demonstrated changes in the microcirculation of blood relative to the control group of animals.[27] The nature of microhemodynamic changes induced by alloxan diabetes is similar to the result obtained for modelled pancreatic gland reperfusion with 5 min ischemia after five days (Fig. 4(b)), which may indicate similar microhemodynamic disorders caused by the development of these pancreatic pathologies.

3.2. *Histological analysis*

The results of the histological analysis showed that in the group with 5 min of ischemia, pancreatic tissue appeared in the edema of the stroma, uneven blood vessel filling, single hemorrhages, the phenomenon of separation, and small foci of necrosis occurred. In a group with 20 min of ischemia, half of the animals died from pancreatonecrosis on the third and fourth day of the experiment. Among the surviving animals, histologically, along with circulatory disturbances, leukostasis was observed with leukodiapedesis in the stroma, the development of common foci of necrosis, which indicates the development of AP.

3.3. *Measurement of the optical properties of the pancreas*

Figures 6–9 show optical properties of the rat pancreatic tissue calculated using IMC software from the measured diffuse reflectance, total and collimated transmittance. The spectra of the absorption coefficient (Fig. 6), the reduced scattering coefficient (Fig. 7), the scattering coefficient (Fig. 8), and the scattering anisotropy factor (Fig. 9) for the tissue in norm and after 20 min-ischemia in five days from the beginning of the experiment are obtained.

Figure 6 presents the wavelength dependence of the absorption coefficient of the pancreatic tissue. The vertical lines correspond to the values of SD, which is determined as follows: $\mathrm{SD} = \sqrt{\sum_{i=1}^{N} (\bar{\mu}_a - \mu_{ai})^2 / N(N-1)}$, where $N = 10$ is the number of the measured tissue samples, μ_{ai} is the absorption coefficient of each sample, and $\bar{\mu}_a$ is the mean value of the absorption coefficient for

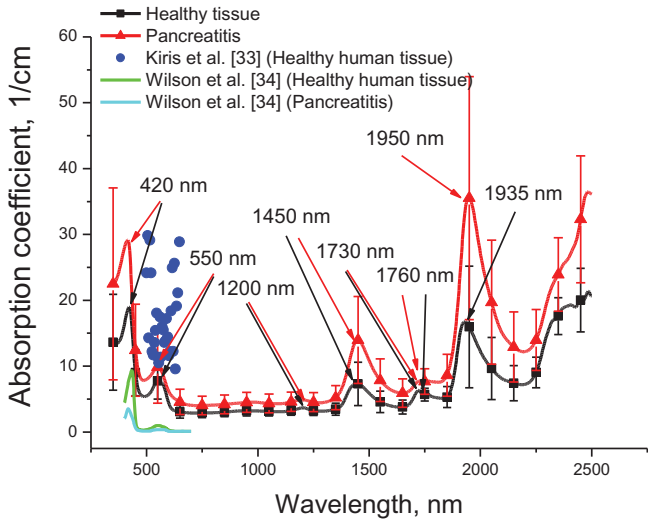

Fig. 6. The spectral dependence of the absorption coefficient of the pancreatic tissue measured for the tissue in norm (black line) and after 20 min-ischemia in five days from the beginning of experiment (red line). The vertical lines show the SD values. The blue circles correspond to μ_a of human healthy tissue from Ref. 33; the green line corresponds to μ_a of human healthy tissue[36] and cyan line corresponds to μ_a of pancreatitis.[33]

each wavelength, which is calculated as $\sum_{i=1}^{N} \mu_{ai}/N$. The absorption spectra clearly show the absorption bands of water with peaks at 1450 and 1935 nm (healthy tissue) and at 1450 and 1950 nm (pancreatitis)[34–37] and hemoglobin with peaks at 420 and 550 nm, which indicates its deoxygenated form.[38]

The red shift of the water band from 1935 nm (H-bonded OH groups with energetically unfavored bond angles[36]) to 1950 nm is associated with tighter bonds of water molecules with proteins[36,37] at pancreatitis. At the same time, for the water band with a maximum at 1450 nm (the first overtone of O–H stretching[39]), the red shift is not observed that was confirmed by data presented in Ref. 36. The absorption band of water with a maximum at 975 nm (the vibrational overtone of the O–H bond[34,35,39]) is not observed in the absorption spectrum of the pancreatic tissue, due to its low intensity. The peak with a maximum value at 1200 nm is the combination of water absorption bands with a maximum value at 1180 nm (the vibrational overtone of the O–H bond[39]) and the lipid absorption band with a maximum value at 1210 nm (the second overtone of C–H stretching[39,40]). The lipid absorption bands with maxima at 1730 and 1760 nm are associated with the first overtone of C–H stretching.[39,40] The observed increase in absorption in the region above 2200 nm is the short wavelength wing of the water absorption band with a maximum at 2950 nm.[30,41,42] Increasing the SD in the range of the absorption bands is connected with differences in the blood, lipids and water content for different tissue samples.

For comparison, Fig. 6 shows the experimental data presented in Refs. 32 and 36. One can see that absorption coefficient values obtained by Kiris *et al.*[32] exceed the values obtained in this study, while Wilson *et al.*[36] show smaller values of absorption coefficient. These differences can be explained by differences in structural and morphological features of the investigated tissues (Kiris *etal.*[32] and Wilson *et al*[36] investigated human pancreatic tissues) and by differences in methods of experimental data processing. For example, the optical characteristics in Ref. 32 were reconstructed using the inverse adding-doubling method[43] that, in principle, can be a cause of overestimation of the absorption coefficient[44,45] and in Ref. 36 using an empirical model[46] previously developed for modeling of reflectance spectra measured using a probe with small source-detector separation.

In Fig. 6, it is well seen that the absorption coefficient of tissue samples with pancreatitis is bigger than that of the control samples. This may be due to edema[47] and extended extravasation of blood (RBCs), i.e., leakage of blood or any fluid from the vessels into the surrounding tissues caused by inflammation,[48] as a severe AP may be accompanied by shock, sepsis, metabolic disturbances, bleeding into the gastrointestinal tract, disseminated intravascular clotting, and multiorgan insufficiency.[48]

The reduced scattering spectra of the tissues under study in the region from 350 to 1300 nm gradually decrease towards longer wavelengths, which are generally consistent with the characteristic of the spectral behavior of the scattering characteristics of biological tissues.[49–52] However, in the region of hemoglobin Soret absorption band (420 nm) and starting from 1300 nm with increasing wavelength, the spectral behavior of the reduced scattering coefficient becomes nonmonotonic in the region of the water absorption bands. The observed peaks of the reduced scattering coefficient can be associated with the influence of the imaginary part of the complex refractive index of the scattering centers (erythrocytes from residual blood and hydrated cell components).[29,30,53] The similar

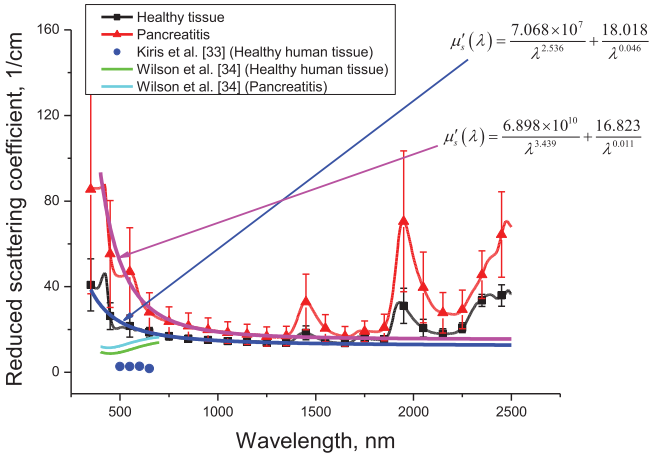

Fig. 7. The spectral dependence of the reduced scattering coefficient of the pancreatic tissue measured for the tissue in norm (black line) and after 20 min-ischemia in five days from the beginning of experiment (red line) and its approximation by power functions (blue and magenta lines). The vertical lines show the SD values. The blue circles correspond to μ_s' of human healthy tissue[32]; the green line corresponds to μ_s' of human healthy tissue,[33] and cyan line corresponds to μ_s' of pancreatitis.[33]

behavior of the reduced scattering coefficient in the region of hemoglobin absorption bands was observed in Ref. 54.

Figure 7 shows the approximations of the wavelength dependence of the reduced scattering coefficient by the sum of power functions $(\mu_s'(\lambda) = A/\lambda_1^w + B/\lambda^{w_2})$, where λ is the wavelength and w is the wavelength exponent. The wavelength exponent characterizes the mean size of the tissue effective scatterers and defines spectral behavior of their scattering properties.[49–51] The first term reflects the spectral behavior associated with small, so-called Rayleigh (or Rayleigh–Gans) scatterers and the second with large, so-called Mie, scatterers.,[52] In Fig. 7 it is well seen that in the spectral range from 600 to 1300 nm, these power functions well approximate the experimental data. Obtained values of the wavelength exponent are 2.536 and 0.046 for the healthy tissue and 3.439 and 0.011 for pancreatitis, respectively, which are the typical ones for many tissues.[53,55]

Observed changes in Rayleigh–Gans and Mie fractions of the tissue scatterers, i.e., increasing w_1 from 2.536 for healthy tissue to 3.439 for pancreatitis and decreasing w_2 from 0.046 for healthy tissue to 0.011 for pancreatitis can be explained by structural and morphological changes in the pancreas during pancreatitis development. For example, increase of w_1 (i.e., decreasing mean size of small effective scatterers) can be associated with pancreas damage and development of common foci of necrosis (see Section "Histological analysis"). In its turn, decrease of w_2 (i.e., increasing mean size of Mie scatterers) deals with extravasation of blood (RBCs) from the vessels into the surrounding tissues[48] and therefore appearance of the large-sized scatterers (blood erythrocytes, vessel walls, etc.).

Figure 7 shows the experimental data presented in Refs. 32 and 36. One can see that reduced scattering coefficient values obtained by Kiris *et al.*[32] and Wilson *et al*[36] are less than the values obtained in this study. These differences can be explained by differences in structural and morphological features of the investigated tissues and by differences in methods of experimental data processing. However, in spite of these differences, data presented by Wilson *et al.*[33] confirm the results obtained in our study, i.e., increasing scattering at pancreatitis.

In Fig. 8, it is seen that, as in the case of the reduced scattering coefficient (see Fig. 7), an increase in light scattering is observed in pancreatitis.

Figure 8 shows the approximation of the wavelength dependence of the scattering coefficient of healthy pancreatic tissue and pancreatitis by the power functions $\mu_s(\lambda) = 171.037/\lambda^{0.098}$ and $\mu_s(\lambda) = 877.937/\lambda^{0.267}$, respectively. It can be seen that, in general, these functions well approximate the experimental data in an entire spectral range.

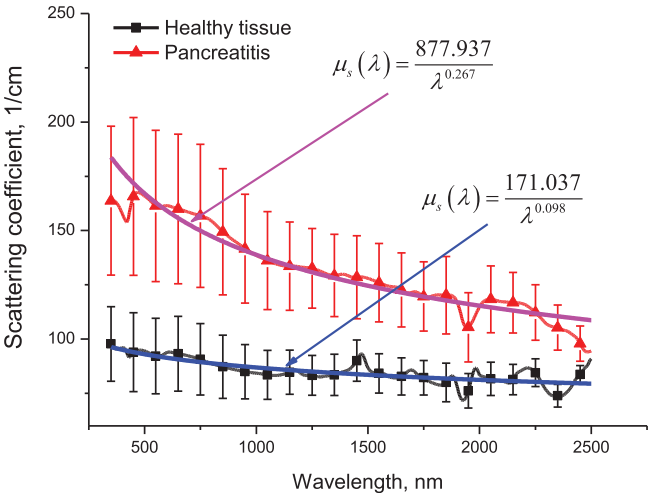

Fig. 8. The spectral dependence of the scattering coefficient of the pancreatic tissue measured for the tissue in norm (black line) and after 20 min-ischemia in five days from the beginning of experiment (red line) and its approximation by a power law (blue and magenta lines). The vertical lines show the SD values.

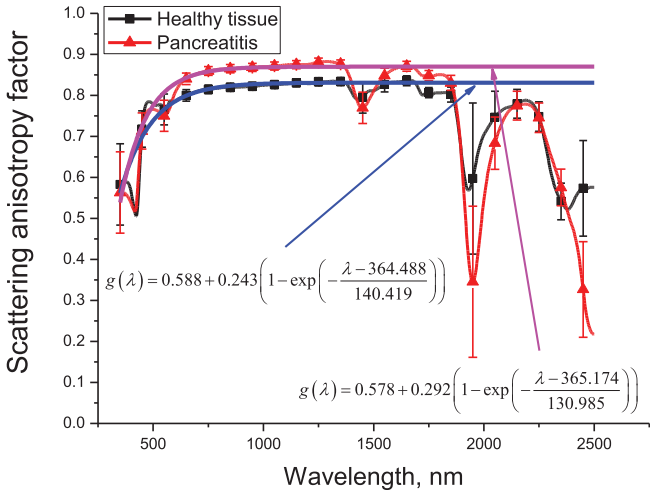

Fig. 9. The wavelength dependence of the scattering anisotropy factor of the pancreatic tissue measured for the tissue in norm (black line) and after 20 min-ischemia in five days from the beginning of experiment (red line) and its approximations (blue and magenta lines). The vertical lines show the SD values.

Comparison of their wavelength exponents shows that at pancreatitis, the mean size of the effective scatterers decreases.

Figure 9 shows the wavelength dependence of scattering anisotropy factor of healthy pancreatic tissue and pancreatitis by the functions $g(\lambda) = 0.588 + 0.243(1 - \exp(-\frac{\lambda - 364.488}{140.419}))$ and $g(\lambda) = 0.578 + 0.292(1 - \exp(-\frac{\lambda - 365.174}{130.985}))$, respectively. The experimental data in the 600–1300 nm spectral region are well approximated by these functions, and the analysis carried out in Refs. 52 and 56 suggests that in the visible region, the shape of the scattering anisotropy factor spectrum is influenced by both small and large particles, while in the NIR region, the main contribution is made only by large enough scatterers, as evidenced by the growth of g with the wavelength increase. In the 1300–2500 spectral range, we observe a decrease in g with sharp dips in the regions of water absorption bands, which is explained by the influence of the imaginary part of the complex refractive index of both the scatterers and the surrounding medium. Such behavior agrees with the experimental data presented in Refs. 29, 30, 56–58 and theoretical calculations presented in Refs. 59 and 60. The dip in the spectrum of the scattering anisotropy factor in the region of 420 nm is associated with the manifestation of hemoglobin absorption in this spectral region.[61]

Light penetration depth is a very important characteristic for correct determination of the radiation dose in the course of photochemical and photodynamic therapy of various diseases, as well as the dosimetry of optical radiation at laser surgery. In diffusion approximation, the assessment of the depth of light penetration into biological tissue (δ) is performed using the expression: $\delta = 1/\sqrt{3\mu_a(\mu_a + \mu_s')}$.[62] This expression is true when a pencil beam is incident on the surface of the scattering medium, and the diffuse radiant influence is mainly created by diffusely scattered photons. Analysis of the penetration depth of ballistic photons used for imaging in OCT or confocal microscopy can be performed on the basis of the expression: $\delta_c = 1/\mu_t$.[63]

In Fig. 10, the optical penetration depth spectra are presented which have been calculated using the absorption and scattering coefficients, given in Figs. 6 and 8, and the reduced scattering coefficient is shown in Fig. 7. It is clearly seen that pancreatitis development significantly (about in 1.5-fold) decreases the light penetration depth for both diffuse and ballistic photons. The maximal penetration depth at pancreatitis for diffuse photons (600 μm) is observed at the wavelength of 1280 nm, and for ballistic photons (80 μm), it is observed at the wavelength of 2264 nm. In a specific spectral range for photodynamic therapy (600–900 nm) for the individual wavelengths, such as 600, 633, 660, 700, 750, 800, 850, and 900 nm,[53] the penetration depth

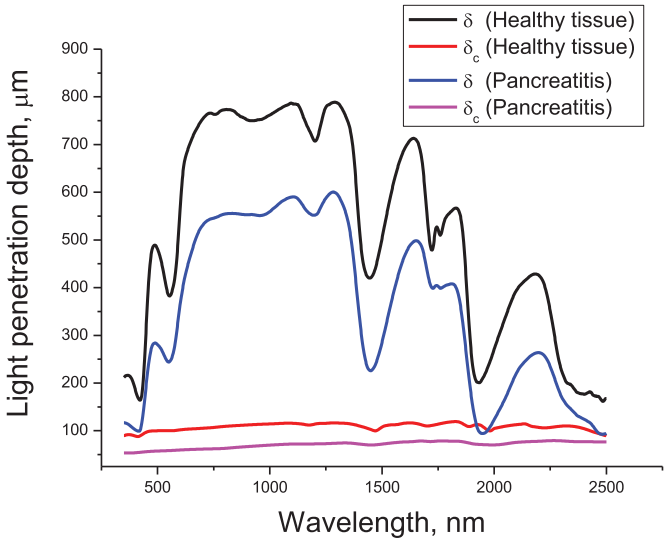

Fig. 10. The optical penetration depth δ and δ_c into the pancreatic tissue calculated for the tissue in norm (black and red lines, respectively) and after 20 min-ischemia in five days from the beginning of experiment (blue and magenta lines, respectively).

at pancreatitis is correspondingly equal to 365, 445, 490, 530, 545, 555, 555, and 550 μm for diffuse photons and 60–66 μm for ballistic photons.

4. Conclusion

The results confirm that LSCI is an effective method for monitoring the microhemodynamics of the pancreas. The method of laser speckle contrast imaging allows one to control the degree of reduction of blood flow in the vessels of the pancreas when creating local ischemia by compression of the main vessels. In the group of animals after 5 min of full ischemia, an increase of PBF velocity in 2–3-fold was found with no developing of pancreatic necrosis determined clinically. After 20 min of full ischemia, there was no significant increase in the rate of PBF, while in five days of the experiment, morphological and clinical signs of pancreatic necrosis appeared. The data obtained confirm the fact that local ischemia and changes in the blood flow velocity of the main vessels cause and provoke acute pancreatitis. This is confirmed also by histological analysis and analysis of changes in the optical properties of the pancreas by the spectral method.

Conflict of Interest

The authors declare that they have no conflict of interest.

Acknowledgments

Authors are thankful to Prof. Elina A. Genina (Department of Optics and Biophotonics of Saratov State University) for her great help in this study. This work was carried out with the financial support of the Project No. 13.2251.21.0009 of the Ministry of Science and Higher Education of the Russian Federation.

References

1. L. Rodrigo (Ed.), Acute Pancreatitis, in *Microcirculatory Disturbances in the Pathogenesis of Acute Pancreatitis*, Chap. 11 pp. 141–159, InTech (2011).
2. R. V. Vashetko, A. D. Tolstoy, A. A. Kurygin, Yu. M. Stoyko, V. B. Krasnorogov, Acute pancreatitis and pancreatic injury, A Guide for Physicians, Peter, pp. 320–321 (2000).
3. A. Warshaw, "A practical guide to pancreatitis," *Gastroenterology* **86**(5), 987 (1984).
4. W. Uhl, A. Warshaw, "IAP guidelines for the surgical management of acute pancreatitis," *Pancreatology* **2**, 565 (2002).
5. M. D. Menger, H. Bonkhoff, B. Vollmar, "Ischemia-reperfusion-induced pancreatic microvascular injury. An intravital fluorescence microscopic study in rats," *Dig. Dis. Sci.* **41**(5), 823 (1996).
6. V. Doblhoff-Dier, L. Schmetterer, W. Vilser, G. Garhöfer, M. Gröschl, R. Leitgeb, R. Werkmeister, "Measurement of the total retinal blood flow using dual beam Fourier-domain Doppler optical coherence tomography with orthogonal detection planes," *Biomed. Opt. Exp.* **5**(2), 630–642 (2014).
7. Y. Huang, Z. Ibrahim, D. Tong, S. Zhu, Q. Mao, J. Pang, W. P. A. Lee, G. Brandacher, J. U. Kang, "Microvascular anastomosis guidance and evaluation using real-time three-dimensional Fourier-domain Doppler optical coherence tomography," *J. Biomed. Opt.* **18**(11), 111404 (2013).
8. Z. Chen, T. E. Milner, X. Wang, S. Srinivas, J. S. Nelson, "Optical doppler tomography: Imaging in vivo blood flow dynamics following pharmacological intervention and photodynamic therapy," *Photochem. Photobiol.* **67**(1), 56–60 (1998).
9. J. D. Briers, "Laser Doppler, speckle and related techniques for blood perfusion mapping and imaging," *Physiol. Meas.* **22**(4), 35–66 (2001).
10. H. Cheng, Q. Luo, S. Zeng, S. Chen, W. Luo, H. Gong, "Hyperosmotic chemical agent's effect on in vivo cerebral blood flow revealed by laser speckle," *Appl. Opt.* **43**(31), 5772–5777 (2004).
11. D. A. Zimnyakov, O. V. Ushakova, D. J. Briers, V. V. Tuchin, Speckle technologies for monitoring and imaging of tissues and tissue-like phantoms, *Handbook of Optical Biomedical Diagnostics, Methods*, 2nd Edition, V. V. Tuchin, Ed., p. 495, SPIE Press, PM263, Bellingham, WA, USA (2016).
12. D. K. Tuchina, P. A. Timoshina, V. V. Tuchin, A. N. Bashkatov, E. A. Genina, "Kinetics of rat skin optical clearing at topical application of 40%glucose: *Ex vivo* and *in vivo* studies," *IEEE J. Sel. Top. Quantum Electron.* **25**(1), 7200508 (2019).
13. A. K. Dunn, "Laser speckle contrast imaging of cerebral blood flow," *Ann. Biomed. Eng.* **40**(2), 367–377 (2012).
14. E. B. Postnikov, M. O. Tsoy, P. A. Timoshina, D. E. Postnov, "Gaussian sliding window for robust processing laser speckle contrast images," *Int. J. Numer. Meth. Biomed. Eng.* **35**(4), e3186 (2019).
15. H. Cheng, Q. Luo, S. Zeng, S. Chen, J. Cen, H. Gong, "Modified laser speckle imaging method

with improved spatial resolution," *J. Biomed. Opt.* **8**(3), 559–564 (2003).
16. D. A. Zimnyakov, A. B. Pravdin, L. V. Kuznetsova, V. I. Kochubey, V. V. Tuchin, "Peculiarities of the diffusion of light in a dense random medium near the edge of fundamental absorption band," *J. Opt. Soc. Am. A* **24**, 711–723 (2007).
17. P. A. Dyachenko, D. A. Alexandrov, A. B. Bucharskaya, V. V. Tuchin, Speckle-contrast imaging of pathological tissue microhemodynamics in the development of various diabetes models, *Prog. Biomed. Opt. Imag. Proc. SPIE* **11457** (2020).
18. E. I. Galanzha, G. E. Brill, Y. Aizu, S. S. Ulyanov, V. V. Tuchin, *Handbook of Optical Biomedical Diagnostics*, pp. 881–938, SPIE Press, Bellingham (2002).
19. D. A. Boas, A. K. Dunn, "Laser speckle contrast imaging in biomedical optics," *J. Biomed Opt.* **15**(1), 011109 (2010).
20. S. Yuan, A. Devor, D. A. Boas, A. K. Dunn, "Spatial extent of oxygen metabolism and hemodynamic changes during functional activation of the rat somatosensory cortex," *Appl. Opt.* **44**, 823, 1830 (2005).
21. Z. Wang, Q. Luo, H. Cheng, W. Luo, Q. Lu, "Blood flow activation in rat somatosensory cortex under sciatic nerve stimulation revealed by laser speckle imaging," *Nat. Sci.* **13**(7), 522–527 (2003).
22. J. D. Briers, S. Webster, "Laser speckle contrast analysis (LASCA): A non-scanning, full-field technique for monitoring capillary blood flow," *J. Biomed. Opt.* **1**(2), 174–179 (1996).
23. Y. Atchia, H. Levy, S. Dufour, O. Levi, "Rapid multiexposure *in vivo* brain imaging system using vertical cavity surface emitting lasers as a light source," *Appl. Opt.* **52**(7), 64–71 (2013).
24. K. Khaksari, S. J. Kirkpatrick, "Laser speckle contrast imaging is sensitive to advective flux," *J. Biomed. Opt.* **21**(7), 076001 (2016).
25. K. Khaksari, S. J. Kirkpatrick, "Combined effects of scattering and absorption on laser speckle contrast imaging," *J. Biomed. Opt.* **21**(7), 076002 (2016).
26. V. V. Tuchin, A. N. Bashkatov, E. A. Genina, V. I. Kochubey, V. V. Lychagov, S. A. Portnov, N. A. Trunina, D. R. Miller, S. Cho, H. Oh, B. Shim, M. Kim, J. Oh, H. Eum, Y. Ku, D. Kim, Y. Yang, "Finger tissue model and blood perfused skin tissue phantom," *Proc. SPIE* **7898**, 78980Z (2011).
27. P. A. Timoshina, A. B. Bucharskaya, D. A. Alexandrov, "Study of blood microcirculation of pancreas in rats with alloxan diabetes by laser speckle contrast imaging," *J. Biomed. Photon. Eng.* **3**(2), 020301 (2017).
28. M. A. Vilensky, O. V. Semyachkina-Glushkovskaya, P. A. Timoshina, Ya. V. Kuznetsova, I. A. Semyachkin-Glushkovsky, D. N. Agafonov, V. V. Tuchin, "Laser speckle imaging of blood microcirculation in the brain cortex of laboratory rats in stress," *Quantum Electron.* **42**(6), 489–494 (2012).
29. A. N. Bashkatov, E. A. Genina, V. I. Kochubey, V. S. Rubtsov, E. A. Kolesnikova, V. V. Tuchin, "Optical properties of human colon tissues in the 350 – 2500 nm spectral range," *Quantum Electron.* **44**(8), 779–784 (2014).
30. A. N. Bashkatov, E. A. Genina, M. D. Kozintseva, V. I. Kochubei, S. Y. Gorodkov, V. V. Tuchin, "Optical properties of peritoneal biological tissues in the spectral range of 350–2500 nm," *Opt. Spectrosc.* **120**(1), 1–8 (2016).
31. K. Celiński, M. Szczerbiński, M. Słomka, B. Kasztelan-Szczerbińska, "The role of adenosine receptors for pancreatic blood flow in caerulein-induced acute pancreatitis," *Rocz. Akad. Med. Białymst.* **48**, 57–60 (2003).
32. T. Kiris, S. Akbulut, A. Kiris, Z. Gucin, O. Karatere, G. B. Ates, H. O. Tabakoglu, "Optical characterization of pancreatic normal and tumor tissues with double integrating sphere system," *Proc. SPIE* **9321**, 932116 (2015).
33. R. H. Wilson, M. Chandra, J. Scheiman, D. Simeone, B. McKenna, J. Purdy, M.-A. Mycek, "Optical spectroscopy detects histological hallmarks of pancreatic cancer," *Opt. Exp.* **17**(20), 17502–17516 (2009).
34. L. Kou, D. Labrie, P. Chylek, "Refractive indices of water and ice in the 0.65- to 2.5-μm spectral range," *Appl. Opt.* **32**(19), 3531–3540 (1993).
35. O. S. Khalil, "Spectroscopic and clinical aspects of noninvasive glucose measurements," *Clin. Chem.* **45**(2), 165–177 (1999).
36. P. L. Walling, J. M. Dabney, "Moisture in skin by near-infrared reflectance spectgroscopy," *J. Soc. Cosmet. Chem.* **40**, 151–171 (1989).
37. D. L. Vandermeulen, N. Ressler, "A near-infrared analysis of water macromolecule interactions: Hydration and the spectra of aqueous solutions of intact proteins," *Arch. Biochem. Biophys.* **199**(1), 197–205 (1980).
38. N. Bosschaart, G. J. Edelman, M. C. G. Aalders, van T. G. Leeuwen, D. J. Faber, "A literature review and novel theoretical approach on the optical properties of whole blood," *Lasers Med. Sci.* **29**, 453–479 (2014).
39. R. H. Wilson, K. P. Nadeau, F. B. Jaworski, B. J. Tromberg, A. J. Durkin, "Review of short-wave infrared spectroscopy and imaging methods for biological tissue characterization," *J. Biomed. Opt.* **20**(3), 030901 (2015).
40. R. Nachabe, van der J. W. A. Hoorn, van de R. Molengraaf, R. Lamerichs, J. Pikkemaat, C. F. Sio,

B. H. W. Hendriks, H. J. C. M. Sterenborg, "Validation of interventional fiber optic spectroscopy with MR spectroscopy, MAS-NMR spectroscopy, high-performance thin-layer chromatography, and histopathology for accurate hepatic fat quantification," *Invest. Radiol.* **47**(4), 209–216 (2012).

41. D. M. Wieliczka, S. Weng, M. R. Querry, "Wedge shaped cell for highly absorbent liquids: infrared optical constants of water," *Appl. Opt.* **28**, 1714–1719 (1989).
42. G. M. Hale, M. R. Querry, "Optical constants of water in the 200 nm to 200 μm wavelength region," *Appl. Opt.* **12**, 555–563 (1973).
43. S. A. Prahl, M. J. C. van Gemert, A. J. Welch, "Determining the optical properties of turbid media by using the adding-doubling method," *Appl. Opt.* **32**, 559–568 (1993).
44. J. H. Torres, A. J. Welch, I. Cilesiz, M. Motamedi, "Tissue optical property measurements: overestimation of absorption coefficient with spectrophotometric techniques," *Lasers Surg. Med.* **14**, 249–257 (1994).
45. D. Zhu, W. Lu, S. Zeng, Q. Luo, "Effect of light losses of sample between two integrating spheres on optical properties estimation," *J. Biomed. Opt.* **12**(6), 064004 (2007).
46. R. Reif, O. A'Amar, I. J. Bigio, "Analytical model of light reflectance for extraction of the optical properties in small volumes of turbid media," *Appl. Opt.* **46**(29), 7317–7328 (2007).
47. X. D. Wang, X. M. Deng, P. Haraldsen, R. Andersson, I. Ihse, "Antioxidant and calcium channel blockers counteract endothelial barrier injury induced by acute pancreatitis in rats," *Scand. J. Gastroenterol.* **30**(11), 1129–1136 (1995).
48. G. Wallner, M. Solecki, C. G. Ziemiakowicz, P. Dyndor, R. Maciejewski, "Morphological changes of the pancreas in course acute pancreatitis during treatment with Ulinastatin," *Pol. J. Surg.* **85**(3), 114–122 (2013).
49. S. Yu. Shchyogolev, "Inverse problems of spectroturbidimetry of biological disperse systems: An overview," *J. Biomed. Opt.* **4**(4), 490–503 (1999).
50. J. M. Schmitt, G. Kumar, "Optical scattering properties of soft tissue: A discrete particle model," *Appl. Opt.* **37**, 2788–2797 (1998).
51. R. K. Wang, "Modelling optical properties of soft tissue by fractal distribution of scatterers," *J. Mod. Opt.* **47**, 103–120 (2000).
52. A. N. Bashkatov, E. A. Genina, V. I. Kochubey, V. V. Tuchin, "Optical properties of human skin, subcutaneous and mucous tissues in the wavelength range from 400 to 2000 nm", *J. Phys. D. Appl. Phys.* **38**(15), 2543–2555 (2005).
53. A. N. Bashkatov, E. A. Genina, V. V. Tuchin, Tissue optical properties, *Handbook of Biomedical Optics*, Chap. 5, D. A. Boas, C. Pitris, N. Ramanujam, Eds., pp. 67–100, Taylor & Francis Group, LLC, CRC Press Inc. (2011).
54. N. Honda, K. Ishii, Y. Kajimoto, T. Kuroiwa, K. Awazu, "Determination of optical properties of human brain tumor tissues from 350 to 1000 nm to investigate the cause of false negatives in fluorescence-guided resection with 5-aminolevulinic acid," *J. Biomed. Opt.* **23**(7), 075006 (2018).
55. A. N. Bashkatov, E. A. Genina, V. V. Tuchin, "Optical properties of skin, subcutaneous, and muscle tissues: a review," *J. Innov. Opt. Health Sci.* **4**(1), 9–38 (2011).
56. A. N. Bashkatov, E. A. Genina, V. I. Kochubey, A. A. Gavrilova, S. V. Kapralov, V. A. Grishaev, V. V. Tuchin, "Optical properties of human stomach mucosa in the spectral range from 400 to 2000 nm: Prognosis for gastroenterology," *Med. Laser Appl.* **22**, 95–104 (2007).
57. J.-P. Ritz, A. Roggan, C. Isbert, G. Muller, H. Buhr, C.-T. Germer, "Optical properties of native and coagulated porcine liver tissue between 400 and 2400 nm," *Lasers Surg. Med.* **29**, 205–212 (2001).
58. Y. Du, X. H. Hu, M. Cariveau, G. W. Kalmus, J. Q. Lu, "Optical properties of porcine skin dermis between 900 nm and 1500 nm," *Phys. Med. Biol.* **46**, 167–181 (2001).
59. Q. Fu, W. Sun, "Mie theory for light scattering by a spherical particle in an absorbing medium," *Appl. Opt.* **40**(9), 1354–1361 (2001).
60. W. Sun, N. G. Loeb, B. Lin, "Light scattering by an infinite circular cylinder immersed in an absorbing medium," *Appl. Opt.* **44**(12), 2338–2342 (2005).
61. A. N. Bashkatov, D. M. Zhestkov, E. A. Genina, V. V. Tuchin, "Immersion clearing of human blood in the visible and near-infrared spectral regions," *Opt. Spectrosc.* **98**(4), 638–646 (2005).
62. V. V. Tuchin, *Tissue Optics: Light Scattering Methods and Instruments for Medical Diagnostics*, 3rd Edition, SPIE Press, Washington, Bellingham, Vol. PM254, p. 988 (2015).
63. S. Golovynskyi, I. Golovynska, L. I. Stepanova, O. I. Datsenko, L. Liu, J. Qu, T. Y. Ohulchanskyy, "Optical windows for head tissues in near-infrared and short-wave infrared regions: Approaching transcranial light applications," *J. Biophoton.* **11**(12), e201800141 (2018).